Temperature dependent dynamics transition of intermittent plastic flow in a metallic glass. II. Dynamics analysis

Z. Y. Liu, G. Wang, K. C. Chan, J. L. Ren, Y. J. Huang et al.

Additional information on J. Appl. Phys.

Temperature dependent dynamics transition of intermittent plastic flow in a metallic glass. II. Dynamics analysis

Z. Y. Liu,[1,2] G. Wang,[1,a)] K. C. Chan,[2,a)] J. L. Ren,[3] Y. J. Huang,[4] X. L. Bian,[1] X. H. Xu,[5] D. S. Zhang,[6] Y. L. Gao,[1] and Q. J. Zhai[1]

[1]*Laboratory for Microstructures, Shanghai University, Shanghai 200444, China*
[2]*Department of Industrial and System Engineering, The Hong Kong Polytechnic University, Hong Kong, China*
[3]*Department of Mathematics, Zhengzhou University, Zhengzhou 450001, China*
[4]*School of Materials Sciences and Engineering, Harbin Institute of Technology, Harbin 150001, China*
[5]*Institute of Mechanics, Chinese Academy of Sciences, Beijing 100083, China*
[6]*Department of Mechanics, Shanghai University, Shanghai 200444, China*

By reducing the testing temperatures down to the temperature well below the glassy transition temperature, the serrated flow behaviour during plastic deformation of a Zr-based metallic glass was experimentally investigated and the results were presented in Part I of the present paper. It shows that the yield strength, the plastic deformation ability, the density of shear bands of the metallic glass increase with decreasing temperature. In order to understand the mechanisms for the changes of the mechanical behaviour at low temperatures, in Part II of this study, the stress-time sequence in the plastic strain regime is characterized by a comprehensive dynamical and statistical analysis. The stress-time sequence is found to exhibit a chaotic state at high temperatures (>203 K), whereas a self-organized critical state is obtained at low temperatures (≤203 K) due to the freezing effect. The reasons for the transition between these two distinct spatio-temporal dynamical states are elucidated by investigating the effect of temperature on the deformation units (shear transformation zones) and the elastic interactions between neighbouring shear bands. The results demonstrate that the low temperatures results in an enhancement of the interactions between the elastic strain fields initiated by neighbouring shear bands, which is primarily responsible for the enhanced plasticity of the metallic glass and a dynamics transition. © 2013 AIP Publishing LLC. [http://dx.doi.org/10.1063/1.4815944]

I. INTRODUCTION

In Part I of the present paper, the compression deformation of a $Zr_{41.25}Ti_{13.75}Ni_{10}Cu_{12.5}Be_{22.5}$ (at. %) metallic glass at low temperatures (from 293 K to 123 K) was experimentally revealed. The yield strength and the plastic deformation ability were significantly improved with decreasing temperature. With increasing plastic strain, the density of shear bands was found to increase, and in the plastic regime, the intermittent serrated flow was observed. The amplitude of these serration events gradually decreased from approximately 35 MPa to 4 MPa when the temperature decreased from 293 K to 203 K. Further decreasing temperature to 123 K, the stress fluctuation of serration events was covered by the background noise. To elucidate these mechanical behaviours, in the past decade, tremendous amount of studies were carried out, and several theories were postulated, such as the shear transformation zone (STZ) theory,[1] the free volume theory,[2] concordant shifting region theory,[3] and the potential energy landscape (PEL) theory.[4] These theories can well describe the elastic deformation behaviour,[3] the homogeneously flow behaviour,[4] and the localized inhomogeneously flow behaviour.[1,2] For the serrated flow, it is believed

to be associated with the shear band formation and propagation process.[5] Quantitatively describing this serrated flow is rather difficult because experimental methods cannot directly build up the relationship between the shear bands and the serration events.[6–8] Since that, a phenomenological model was established to schematically examine the correlation between the shear banding and serration events of metallic glasses by analysing the elastic energy aggregation and release in serration events.[9] Since the serrated flow that corresponds to the discrete bursts of plasticity cannot be elucidated using the continuum theory alone,[10,11] some researchers have applied statistical analysis to investigate the serrated flow behaviour.[12–15] Using such a method, two distinct types of dynamical behaviour: self-organized critical (SOC) behaviour and chaotic behaviour,[12,13] have been reported in different metallic glasses. However, the transition mechanism between SOC and chaotic behaviour is still not clear and has yet to be determined. The links between the dynamic behaviours of serrated flow and the deformation unit evolution in the deformation process are absent. Thus, it requires a quantitatively physical mechanism to describe the correlation of the deformation units, serrated flow and shear bands.

In this paper, based on dynamical and statistical analysis of the resultant stress-time series during serrated flow, the dynamics of the serrated flow are characterized in a wide temperature range (293 K to 123 K). Temporal correlation of

a)Authors to whom correspondence should be addressed. Electronic addresses: g.wang@shu.edu.cn and mfkcchan@inet.polyu.edu.hk.

the serration events in the plastic flow regime is characterized by a nonlinear dynamics theory. Spatial interactions between the shear bands are also elucidated by simulating the elastic strain fields at the tip of shear bands. The purpose of the present study is not only to understand how the deformation medium (shear bands and STZs) changes at low temperatures and their effect on the mechanical properties of metallic glasses, but also to better understand how the dynamical behaviour evolution of serrated flow is influenced by the intriguing spatial and temporal interaction between the shear bands.

II. DYNAMICS TRANSITION AT LOW TEMPERATURE

Based on the enlarged experimental stress-time (σ-t) curves at four representative temperatures of 293 K, 223 K,

203 K, and 193 K (Figs. 1(a), 1(c), 1(e), and 1(g)), which have been reported in Part I of the paper, the corresponding quantity of $|d\sigma/dt|$ is plotted in Figs. 1(b), 1(d), and 1(f) to reflect bursts of plastic serration events. The $|d\sigma/dt|$ value as the function of time, t, at 293 K exhibits that time interval, t_n, between any two neighbouring serration events are homogeneous ($t_{n-1} \approx t_n \approx t_{n+1}$) (Fig. 1(b)). Decreasing the temperature to 223 K leads to slightly inhomogeneous time intervals (Fig. 1(d)). Further decreasing temperature to 203 K results in very inhomogeneous time intervals ($t_{n-1} \neq t_n \neq t_{n+1}$) (Fig. 1(f)), suggesting that the serration events at relatively low temperatures ($<$203 K) lack of any typical time scale. This phenomenon indicates a characteristic of SOC behaviour.[16] When temperature continues to decrease, accurate fluctuation of the stress due to the serration events cannot be
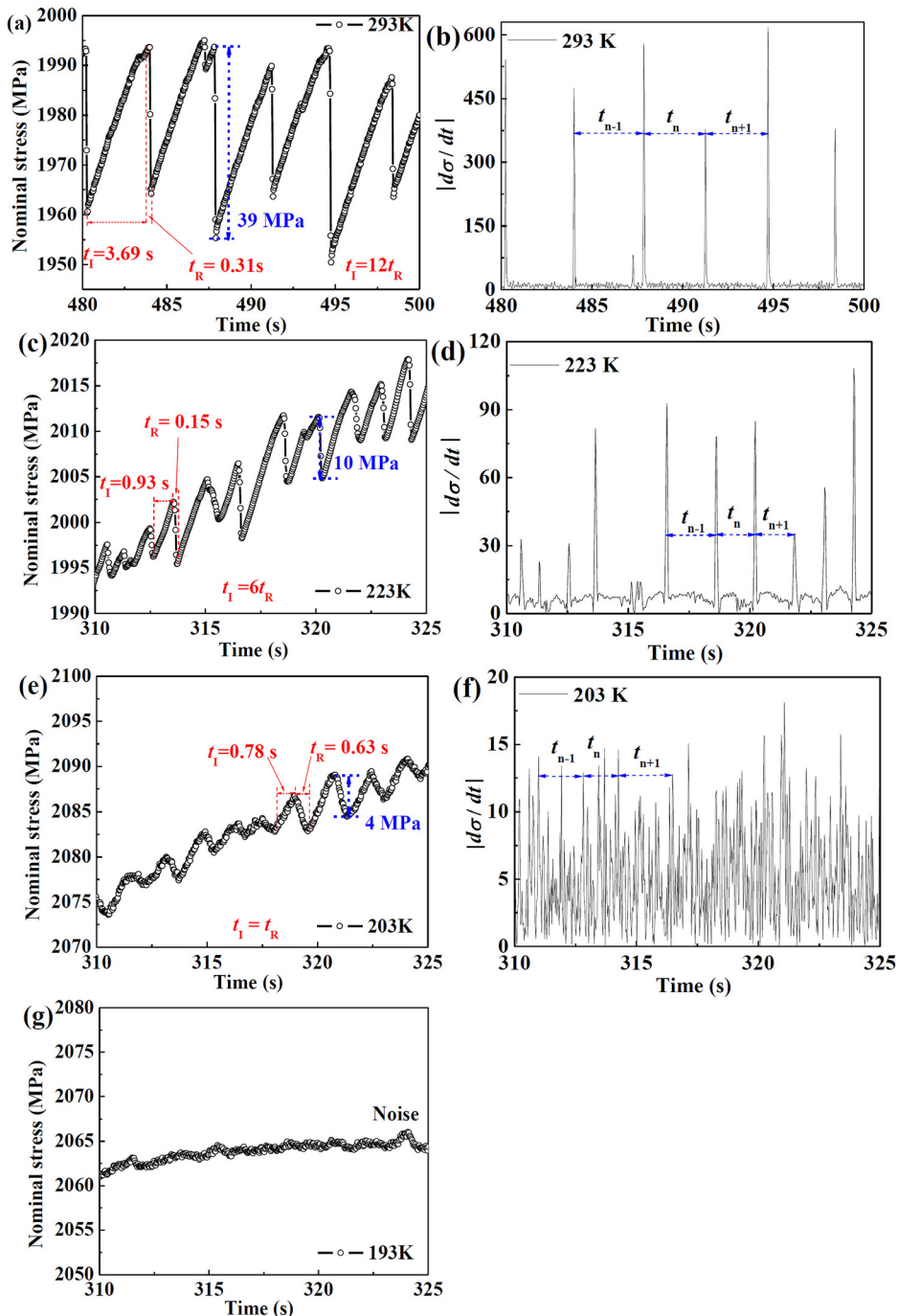

FIG. 1. Enlarged stress-time curves of the $Zr_{41.25}Ti_{13.75}Ni_{10}Cu_{12.5}Be_{22.5}$ metallic at four different temperatures, along with a plot of the corresponding $|d\sigma/dt|$ curves. *Note*: t_n indicates the processing time of one serration event. The $|d\sigma/dt|$ curve at 193 K is not plotted because the background noise covers serration vents.

discerned because of background noise. An average elastic energy accumulation time between two successive drops, t_I, and an average relaxation time, t_R, is representatively marked in Figs. 1(a), 1(c), and 1(e) and also listed in Table I. It is evident that with decreasing temperature, the ratio between the elastic energy accumulation time and the relaxation time, $R \ (= t_I/t_R)$, increases from approximately 11.9 at 293 K to 1.2 at 203 K.

Stress drop in serration events is associated with shear band formation and propagation, which makes it difficult to directly establish quantitative relationships among the serration event, the elastic energy and the shear band number.[11] Moreover, direct observation of the elastic energy relaxation during serration is impossible. Since the amplitude of stress undulation during serration events initially appears to be irregularly and stochastically distributed across the variant strain conditions produced by different loading rates and temperatures,[13,17] mechanistic trends are identified in these distributions by applying dynamic and statistical analyses. Using these methods, a better understanding of the mechanism is achieved despite the characteristic lack of periodicity in intermittent serrated flow behaviour.

Nonlinear dynamics provides a powerful tool to separate the complex behaviour in a nonlinear system into numerous spatio-temporal units in different scales.[18] These units conform a hierarchical structure in which each unit can drive the dynamical system. This hierarchic structure consists of vectors, $\delta u(t)$, and associated Lyapunov exponents, λ_i, indexed by $i = 1, 2, ..., M$, and ordered by decreasing i. Each vector, $\delta u(t)$, represents a particular set of time dependent, infinitesimal, translational perturbations and velocity perturbations. Thus, the dynamic analysis will trace the time dependent vectors and their diverge rate that is associated with the Lyapunov exponent. In the serrated flow of metallic glasses, the stress as a time dependent value is treated as the spatio-temporal unit in the dynamic system. Therefore, according to the analysis method for dynamic systems, the stress signal in each temperature as a time function in the plastic regime is used to further determine the characteristics of serrated flow. In this case, a mathematical model is required to bridge

TABLE I. Mechanical properties of the metallic glass compressed at different temperatures. T is temperature, G_{0T} is shear modulus, τ_{CT} is critical shear stress, γ_{CT} is critical shear strain, L_Y is the largest Lyapunov exponent, τ is the time delay, m is the embedding dimension, D_S is the average interval space between neighbouring shear bands, t_I is average elastic energy accumulation time, t_R is average elastic energy relaxation time and $R = t_I/t_R$. The experimental process was summarized in Part I of the paper.

T (K)	G_{0T} (GPa)	τ_{CT} (MPa)	γ_{CT}	D_S (μm)	t_I (s)	t_R (s)	R	τ	m	L_Y
293	32.1	927	0.0289	~100	1.79	0.15	11.9	25	8	0.011
273	32.7	931	0.0285	~100	1.81	0.16	11.3	60	10	0.025
223	33.7	966	0.0287	~70	1.98	0.24	8.3	2	6	0.008
213	33.8	1035	0.0306	~60	1.17	0.60	2.0	37	10	0.002
203	34.0	1053	0.0310	~40	0.76	0.62	1.2	31	10	−0.001
193	34.2	1023	0.0299	~30	/	/	/	39	9	−0.004
183	34.4	1089	0.0317	~30	/	/	/	/	/	/
173	34.5	1090	0.0316	~20	/	/	/	/	/	/
123	35.2	1180	0.0335	~20	/	/	/	/	/	/

the missing part between the mathematical description of the dynamical system and the experimental stress-time series in the metallic glass. Thus, a phase space concept is introduced to deterministically model the possible states of the dynamical system.[19] Phase space reconstruction is a primary method of analysing the stochastic time series of $\{\sigma(t), (t = 1, 2, ..., N)\}$ (where $\sigma(t)$ is the stress at the time t, as shown in Fig. 1), which builds a proxy of the observed dynamic states.[19] The phase space reconstruction firstly embeds the given stress-time sequence $\{\sigma(t), (t = 1, 2, ..., N)\}$, into a higher dimensional space to reveal all the information hidden in this sequence using a time delay technique.[20] For the time series of $\{\sigma(t), (t = 1, 2, ..., N)\}$, choosing an appropriate embedding dimension, m, and a time delay, τ, are the necessary conditions for the phase space reconstruction. The mutual information method, which is the mainstream approach that is able to obtain the exact time delay, is used to measure the nonlinear correlation of the time series.[20] The mutual information for two random variables is a quantity that measures the mutual dependence of each of two random variables. The time delay, τ, as the mutual information of two variables taking the minimum value at the first time, is selected as the optimal time delay for phase space reconstruction, which is calculated as listed in Table I. Subsequently, because the Cao-method can avoid the influence of the noise on the stress signal, which makes the result more accurate and is an effective method for the small quantity of data, we choose it to calculate the embedding dimension that are also listed in Table I.[21] The embedding dimension, m, is chosen, when the distances for the nearest two points no longer change in the m and $m + 1$ space, to accurately reflect the structure of the dynamic system. This produces a reconstructed phase space spanned by a m-dimension vector of $Y(t_i) = \{\sigma(t_i), \sigma(t_i + \tau), ..., \sigma(t_i + (m - 1)\tau), t_i = 1, ..., [N - (m - 1)\tau]\}$, where t_i is the ith evolution time. Based on this reconstructed phase space, Wolf's method is used to calculate the largest Lyapunov exponents.[22] Set the initial point, $Y(t_0)$, and its nearest neighbour point, $Y_0(t_0)$ (the distance between these two points is L_0), after a period of time, these two points evolve to be $Y(t_1)$ and $Y_0(t_1)$, respectively, and the distance of these two points develops to be $L_0' = |Y(t_1) - Y_0(t_1)| > \omega$, where ω is a constant slightly larger than the minimum distance of each two points in the phase space. Then, around the point of $Y(t_1)$, its nearest neighbouring point is taken as $Y_1(t_1)$. The distance between $Y(t_1)$ and $Y_1(t_1)$ is L_1. Tracking the evolution of $Y(t_1)$ and $Y_1(t_1)$ to get $L_1' = |Y(t_2) - Y_1(t_2)|$, and repeating the above process until the m-dimensional vector, $Y(t_i)$, reaches the end of the time series. The iteration number for this evolution tracking is M. Then the largest Lyapunove exponent, λ, can be calculated to be[23]

$$\lambda = \frac{1}{t_M - t_0} \sum_{i=0}^{M} \ln \frac{L_i'}{L_i}. \tag{1}$$

According to Eq. (1), the largest Lyapunov exponent implies an average exponentially diverging rate of the two trajectories in the phase space.[23] A positive Lyapunov exponent

suggests that the trajectories in the phase space diverge at an exponential rate (at least) in some directions. In other words, the neighbouring points, no matter how close, will diverge, which is characteristic of a chaotic state. It is obvious that chaotic state describes the evolution of a dynamic system that is very sensitive to initial conditions. Small perturbation in initial conditions yields fast diverging evolution trajectories.[18] A negative Lyapunov exponent suggests that the trajectories in the phase space converge at an exponential rate, characteristic of a dissipative or non-conservative dynamic system. Such systems exhibit asymptotic stability, in which smaller negative exponents generate greater stability.[21] The largest Lyapunov exponents of the metallic glass strained at different temperatures are listed in Table I. Clearly, the deformation occurring between 293 K and 213 K represents a chaotic state, while deformation occurring at less than 203 K represents a stable state.

Based on these dynamic approaches, statistical analysis is conducted to further characterize the stochastic serration events in this metallic glass. Since extremely localized shear flow occurs in the shear bands, thus inducing stress drops in the serration events, the shear avalanche size can be represented by the stress drop.[12] The statistical distribution of the shear drops forms a unique profile of shear avalanche sizes that are distinct to each plastically strained metallic glass, essentially like a fingerprint for each material.[24] According to previously described methods,[12] after removing the serration events resulted from the noise from testing system, the stress drop is subjected to normalization, resulting in the statistical distributions of the normalized stress drop, S, shown in Fig. 2. From 293 K to 213 K, the normalized stress drops reveal peaked distributions, suggesting chaotic behaviour.[25] Further decreasing temperature generates a power-law distribution of stress with an exponent of 1.61 ± 0.19, as shown in the inset of Fig. 2. This suggests that SOC behaviour occurs in the stable state.[12] These statistical distributions for stress drop are consistent with Lyapunov exponent calculations.

Dynamic analysis of the serrated flow provides a mathematical index reflecting the shear banding temporal interference.[13] It then requires a physical mechanism to link the mathematical analysis and the experimental phenomena. The structural origination of the deformation in metallic glasses is attributed to deformation unit operation.[1,2] In the elastic
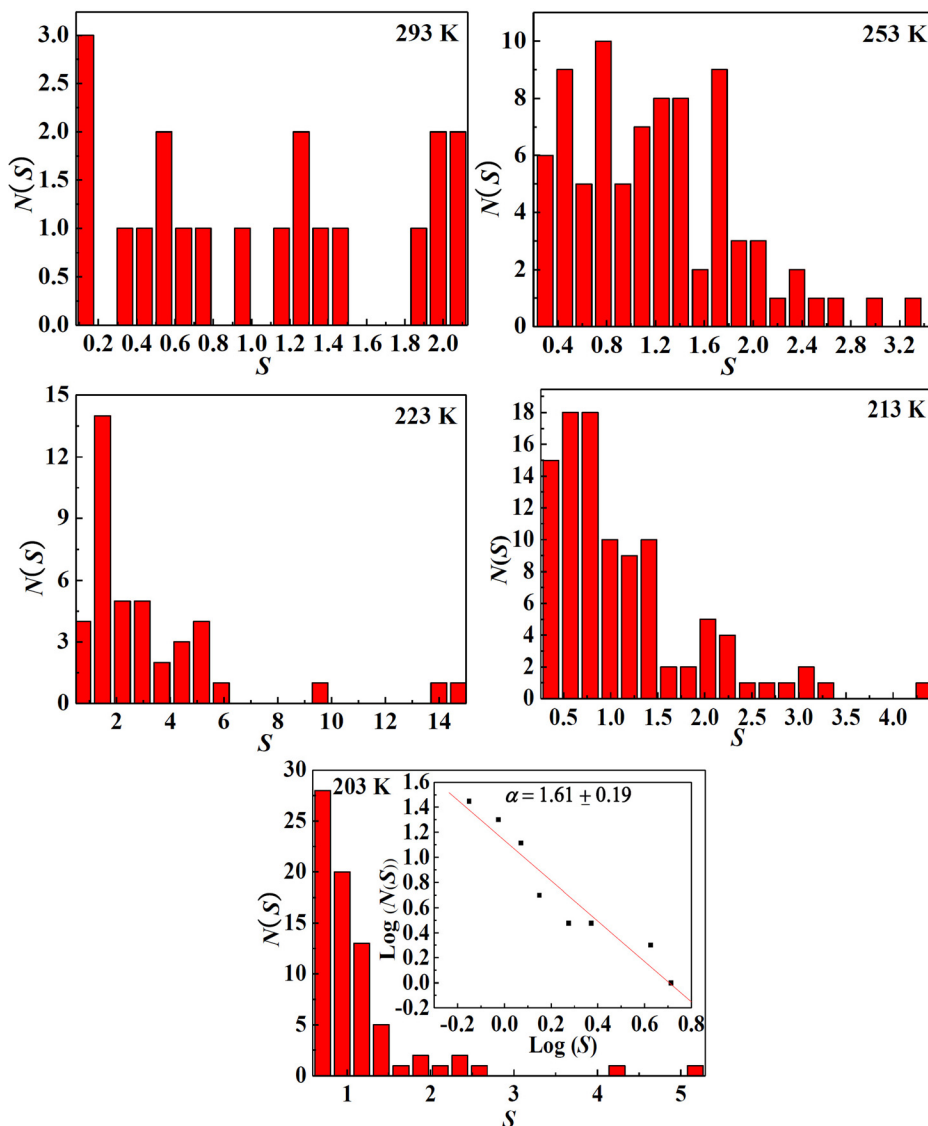

FIG. 2. Statistical distribution of the stress drop, $N(s)$, of the $Zr_{41.25}Ti_{13.75}Ni_{10}Cu_{12.5}Be_{22.5}$ metallic glass deformed at different temperatures. The inset shows the power-law distribution of the stress drop at 203 K.

deformation stage, the elastic stress can drive atoms concordantly shifting, and form a concordant region.[3] With the elastic stress increasing, more atoms can participate in a concordant shift, resulting an expansion of the concordant shifting region. After yielding, this expansion possibly approaches a jamming state because of the elastic field interaction between neighbouring concordant regions.[26] The expansion of the concordant region generates a larger internal stress concentration, causing that new flow events, such as STZs, can be more easily activated.[27] Therefore, the growth of the concordant region in the elastic regime can effectively activate the shear banding operation. In the plastic deformation stage, the elastic stress increase in each serration event also corresponds to the concordant region change in a smaller scale as compared to that happens in the elastic deformation stage. The concordant shifting region model elucidates the idea that atoms in glassy phase shifting concordantly could form a jamming state. A "pining" stress required for operating the concordant region is therefore increased with loading time.[28] When the stress is increased to be larger than the yield stress, flow event operates and the shear banding can slide a given distance. Thus, intermittent serrated flow is formed due to these concordantly shifting regions collectively operating.

Accordingly, the time-dependent stress value that is used in the dynamic analysis reflects the shear bands temporal interaction. The chaotic behaviour at higher temperature (>203 K) correspondingly shows large amplitudes in serration events. They suggest that the elastic energy accumulation time is much larger than the stress drop time, i.e., the elastic energy relaxation time. Thus, the elastic energy in each serration event can be quickly relaxed and there is no temporal correlation between neighbouring serration events, which could result in the chaotic behaviour.[29] In the SOC state, the elastic strain accumulation time is comparable with the relaxation time, suggesting that the elastic energy in the serration events cannot be fully relaxed during this limited time (Table I). This can enhance the interference between the elastic energy stored in neighbouring serration events in the temporal space. Thus, new shear bands are formed in the field of the unrelaxed elastic energy, which possibly forms a hierarchy of length scales in the shear bands,[29] leading to the SOC behaviour. However, the dynamic and statistic analysis, and the elastic accumulation and relaxation times observation cannot provide a clear picture to elucidate the spatial interaction between shear bands. As such, more work has to be done to further support the above dynamics transition analysis.

III. STZ VOLUME AND SPATIAL INTERACTION BETWEEN SHEAR BANDS AT LOW TEMPERATURES

The potential landscape theory of liquids provides an energic conceptualization framework for bridging elastic deformation and plastic flow in metallic glasses.[26] In this theory, the flow of metallic glasses is modelled as a movement of atoms between inherent states and across energy barriers.[30,31] The activation energy for this barrier, W, can be expressed as $W = (8/\pi^2)\gamma_C^2 G\Omega$, where G is the shear modulus, Ω is the effective shear transition zone (STZ) volume, and γ_c is a critical shear strain for metallic glasses, which

was found to be a constant (0.036) for metallic glasses at room temperature.[2,32] Accordingly, the activation energy of atoms cooperative motion across such barriers is dominated by the shear modulus and the activation volume of STZ.

The activation volume of STZ can be calculated by[31] $\Omega = \frac{kT\ln(\omega_0/C\dot{\gamma})}{4RG_{0T}\gamma_C^2\varsigma(1-\tau_{CT}/\tau_{C0})^{3/2}}$, where $\ln(\omega_0/C\dot{\gamma}) \approx 30$; $R \approx 0.25$; $\varsigma \approx 3$; T is the environmental temperature; k is Boltzmann constant (1.381×10^{-23} J/K); τ_{C0} is the yield shear stress at 0 K; G_{0T} is the shear modulus at the temperature of T. According to the shear modulus as the function of temperature shown in Part I of present paper, the shear modulus at 0 K can be deduced to be 35.3 GPa and the critical shear strain at 0 K, γ_{C0}, is 0.036,[31] the τ_{C0} value is approximately 1271 MPa. The critical shear stress at different temperatures can be calculated by $\tau_{CT} = \sigma_{FT}\sin\theta_T\cos\theta_T$,[33,34] where σ_{FT} and θ_T are the fracture stress and the fracture angle at different temperatures, respectively. The fracture angle and the fracture stress were determined in Part I of present paper. Thus, the activation volume of STZ is calculated as a function of temperature, as shown in Fig. 3. For decreasing temperatures from 293 K to 203 K, the volume of STZ slightly increases from 13.3 nm^3 to 18.7 nm^3. Subsequently, the volume increases dramatically to 104.8 nm^3 as the temperature further decreases to 123 K. The volume of STZ and shear modulus changes result in the activation energy of STZ correspondingly increasing (Fig. 3).

Activation energy of STZs increases at low temperatures, indicating that deformation requires more energy than is required at room temperature. Thus, more elastic energy must be accumulated in the elastic regime to compensate for the incremental activation energy as the temperature decreases. The yield strength and elastic energy (elastic modulus) resultantly increase, which is consistent with previous reports.[35,36] Simultaneously, increasing the STZ size significantly enhances the stress concentration around the STZs,[27] further enabling multiple shear band formation. As expected, the density of the shear bands increases with temperature.

Shear localization can be attributed to STZs aggregation[7] that activates a stress concentration, resulting in the formation of an elastic strain field at the localization point.[37–39] This elastic shear strain field can expand to approximately 600 μm in the direction perpendicular to the loading
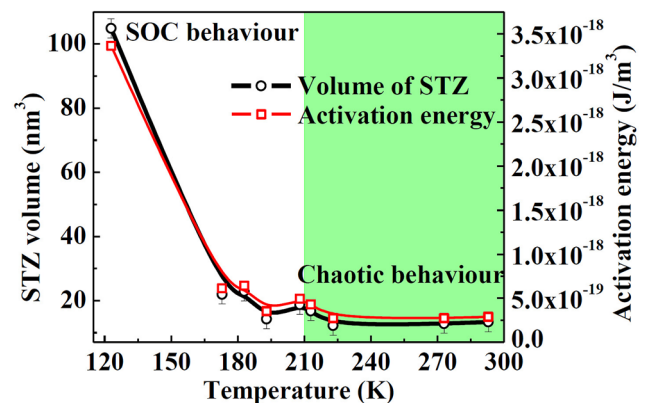

FIG. 3. The volume of STZ and its activation energies as functions of temperature.

direction. Several shear bands are covered in this range because the maximum average interval space is only 155 μm at 293 K (Table I), indicating that the elastic shear strain fields resulting from the neighbouring shear bands must mutually interact. As the temperature decreases, the average interval space decreases to approximately 32 μm and 20 μm at 183 K and 123 K, respectively (Table I). A larger density of shear bands can be expected to enhance these interactions. In light of the interaction between the long-range elastic stress fields generated by dislocations in crystalline materials, these interactions may result in significant work hardening.[40] As a result, interactions between the elastic strain field around the shear band tip or the shear localization point must distort the atomic bonds, causing alterations in the local shear stress.

To further quantitatively describe the interaction between neighbouring shear bands, we discuss it in the framework of elastic mechanics. The elastic strain field can be simplified and expressed as a semi-infinite elastic body,[41] demonstrated in the schematic plot in Fig. 4(a). In this sketch, two arrows represent the shear band tips that activate the underlying local elastic strain field. The interval space between these two neighbouring shear bands is denoted by $2x_0$. Thus, the interaction between the shear bands can be treated as the superposition of two elastic strain fields, and the shear stress can be expressed as

$$\tau_{xy} = \frac{3P}{2\pi} z^2 \left\{ \frac{x + x_0}{[(x + x_0)^2 + z^2]^{5/2}} + \frac{x - x_0}{[(x - x_0)^2 + z^2]^{5/2}} \right\}, \quad (2)$$

where P is the load (assumed to be 500 N, corresponding to the maximum load in our DSCM experiment), and z and x values are in respect to the position of one point in the elastic strain field. The z values are 1, 2, and 4 μm according to the dotted line in Fig. 4(a), which represents points in the interaction area. Then, five x values are chosen to reflect the shear stresses along $z = 1$, 2, 4 μm as a function of the interval space, x_0, which is plotted in logarithmic coordinates in Figs. 4(b)–4(d), respectively.

Therefore, when the x_0 value decreases from 85 μm to 10 μm, i.e., the interval space between the shear bands decreases from 170 μm to 20 μm, the shear stress in the interaction area increases approximately 10^5–10^6 times. Referring to Table I, the critical shear stresses at different temperatures, τ_{CT}, are in the range of 1053 ± 126 MPa. This value is marked by a dashed line in Figs. 4(b)–4(d). When the shear stress from Eq. (2) is higher than the critical shear stress (1053 ± 126 MPa), shear banding is activated. According to Fig. 4(b), at the critical shear stress (1053 MPa), a critical interval space between neighbouring shear bands exists at $2x_0 = 46 \mu m$ ($x_0 = 23 \pm 6 \mu m$). The interval spaces between the shear bands in the temperature range from 293 K to 213 K is higher than the critical interval space of 46 μm at the point of $z = 1 \mu m$ (cf. Table I). For temperatures lower than 203 K, the interval space is significantly less than the critical value. This indicates that long-range interactions between the shear bands can significantly improve the shear stress in localized regions, which is caused by a confinement effect of the elastic shear strain fields by two neighbouring shear bands.[42] Thus, localized yielding occurs in a hydrostatic state, as previously described,[43] and the weak shear bands appear in these highly stressed regions associated with small shear banding processes. In this case, elastic energy can be relaxed by the formation of various shear bands in different scales, which generates a hierarchical structure in the length scales. These are manifested as weak traces of the surviving shear bands on
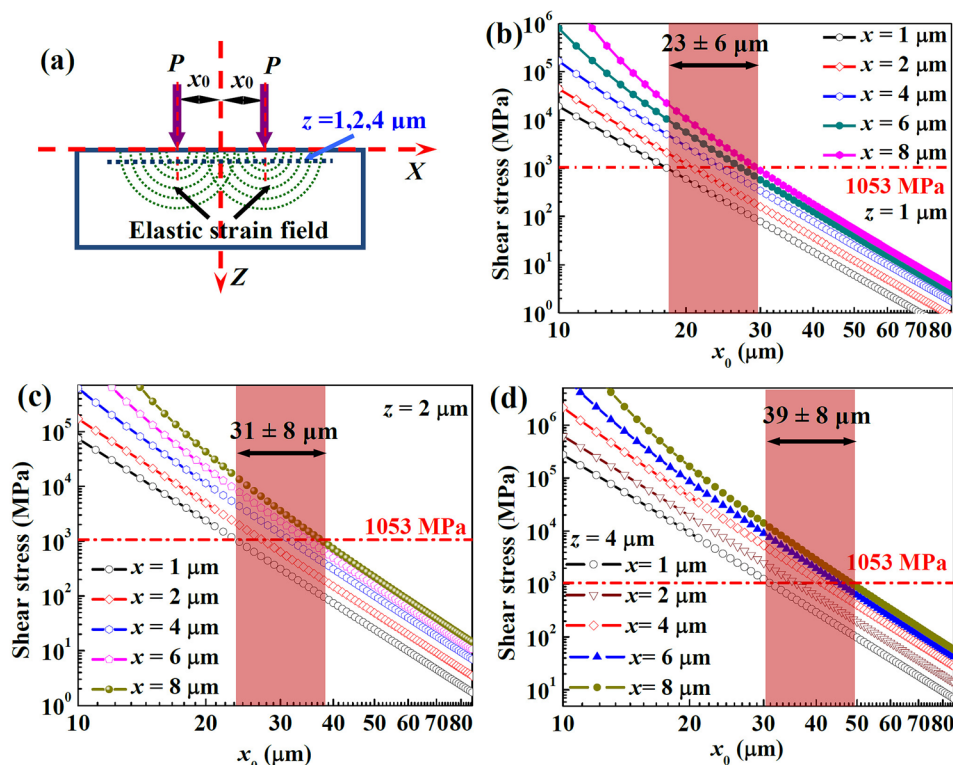

FIG. 4. (a) Sketch illustrating the interference between two neighbouring elastic strain fields. P is the maximum load. Z-axis is the loading direction. x_0 is the half distance between two neighbouring shear bands. (b) The shear stress as a function of the x_0 value at $z = 1 \mu m$. (c) The shear stress as a function of the x_0 value at $z = 2 \mu m$. (d) The shear stress as a function of the x_0 value at $z = 4 \mu m$.

fractured sample surfaces deformed at 203–123 K. As a result, serrated flow behaviour is non-significant or non-existent, as shown in Fig. 1(g), at very low temperatures. Furthermore, the appearance of the shear bands in different length scales, i.e., the hierarchical structure of the shear bands, causes SOC behaviour to be observed.[37]

Just past the shear band tip ($z = 2$ and $4 \mu m$), the critical interval spaces approach $62 \mu m$ and $78 \mu m$ ($x_0 = 31 \pm 8$ and $39 \pm 8 \mu m$) (Figs. 4(c) and 4(d)), respectively. In this case, not only plastic straining occurs at the lower temperatures (≤ 213 K) but also the deformation at the higher temperatures (213 K and 223 K) can elevate the shear stress because the average interval spaces at 213 K ($60 \mu m$) and 223 K ($72 \mu m$) are already smaller than the critical interval spaces ($62 \mu m$ and $78 \mu m$). However, notably, as the z value is increased, the points achieving critical shear yielding become increasingly far from the shear band tips. Meantime, since the points are far away from the shear band tips, the confinement effects produced by interactions between the two shear bands are correspondingly weakened, potentially resulting in failure to produce the conditions necessary for localized yielding. Therefore, weak shear bands are only observed at very low temperatures (≤ 213 K).

IV. CONCLUSIONS

Stochastic stress-time series analysis, i.e., dynamic analysis, as well as statistical analysis show that the dynamics of serrated flow behaviour evolve from the chaotic state to the SOC state when the temperature decreases to less than 203 K. In the chaotic state, the deformation mediums (or units), such as shear bands, evolve in the divergent trajectory, suggesting the shear bands could propagate individually without strong interference and confinement, which is manifested by the large stress amplitude in the serration events. In this case, the dynamic system of the plastic deformation is very sensitive to these stress fluctuations, and the plastic strain ability becomes relative poor. In the SOC state, the strong interaction between shear bands can initiate numerous weak shear bands, leading to a high density of shear bands. The amplitude of stress fluctuation in the serrated flow is therefore reduced, and the dynamic system of the plastic deformation is insensitive to the stress perturbation, leading to a large strain ability.

The experimental results provide a solid evidence to support the dynamic and statistical analysis. Low temperatures freeze the atomic motion of the metallic glass, resulting in more atom participation in deformation units (STZs). This significantly promotes the size and the activation energy required of STZs, which is shown to correspond to higher stress concentrations, thus increasing the quantity (density) of the shear bands. As a result, the interactions between elastic strain fields of neighbouring shear bands are enhanced by the decreased interval space of the shear bands, which promote localized yielding. It will further initiate shear bands in a smaller length scale. The formation of shear bands at different length scales is associated with the hierarchical shear band structure, which is a key factor generating the characteristic transition from chaotic behaviour at high temperatures to

SOC behaviour at very low temperatures. With the understanding of the mechanism of the dynamics transition, it may be able to characterize the elastic energy dissipation more accurately during the intermittent plastic deformation and provide a practicable method to enhance the malleable ability of metallic glasses from the viewpoint of elastic energy accumulation and relaxation.

[1] C. A. Schuh and A. C. Lund, Nature Mater. **2**, 449 (2003).
[2] F. Spaepen, Acta Metall. **25**, 407 (1977).
[3] G. Wang, N. Mattern, J. Bednarčík, R. Li, B. Zhang, and J. Eckert, Acta Mater. **60**, 3074 (2012).
[4] J. Schroers and W. L. Johnson, Phys. Rev. Lett. **93**, 255506 (2004).
[5] D. Klaumünzer, A. Lazarev, R. Maaß, F. H. Dalla Torre, A. Vinogradov, and J. F. Löffler, Phys. Rev. Lett. **107**, 185502 (2011).
[6] F. H. Dalla Torre, D. Klaumünzer, R. Maaß, and J. F. Löffler, Acta Mater. **58**, 3742 (2010).
[7] J. J. Lewandoski and A. L. Greer, Nature Mater. **5**, 15 (2006).
[8] G. Wang, Y. H. Liu, P. Yu, D. Q. Zhao, M. X. Pan, and W. H. Wang, Appl. Phys. Lett. **89**, 251909 (2006).
[9] Y. Q. Cheng, Z. Han, Y. Li, and E. Ma, Phys. Rev. B **80**, 134115 (2009).
[10] A. Portevin and F. Le Chatelier, C. R. hebd. Séanc Acad. Sci. Paris **176**, 507 (1923).
[11] G. Wang, K. C. Chan, L. Xia, P. Yu, J. Shen, and W. H. Wang, Acta Mater. **57**, 6146 (2009).
[12] B. A. Sun, H. B. Yu, W. Jiao, H. Y. Bai, D. Q. Zhao, and W. H. Wang, Phys. Rev. Lett. **105**, 035501 (2010).
[13] R. Sarmah, G. Ananthakrishna, B. A. Sun, and W. H. Wang, Acta Mater. **59**, 4482 (2011).
[14] F. F. Csikor, C. Motz, D. Weygand, M. Zaiser, and S. Zapperi, Science **318**, 251 (2007).
[15] J. Kumar and G. Ananthakrishna, Phys. Rev. Lett. **106**, 106001 (2011).
[16] M. Koslowski, R. LeSar, and R. Thomson, Phys. Rev. Lett. **93**, 125502 (2004).
[17] J. L. Ren, C. Chen, G. Wang, N. Mattern, and J. Eckert, AIP Adv. **1**, 032158 (2011).
[18] E. J. Banigan, M. K. Illich, D. J. Stace-Naughton, and D. A. Egolf, Nat. Phys. **9**, 288–292 (2013).
[19] S. H. Strogatz, *Nonlinear Dynamics and Chaos* (Perseus Books, Cambridge, MA, 1994).
[20] A. M. Fraser and H. L. Swinney, Phys. Rev. A **33**, 1134 (1986).
[21] L. Cao, Physica D **110**, 43 (1997).
[22] A. Wolf, J. B. Swift, H. L. Swinney, and J. A. Vastano, Physica D **16**, 285 (1985).
[23] J. L. Ren, C. Chen, Z. Y. Liu, R. Li, and G. Wang, Phys. Rev. B **86**, 134303 (2012).
[24] B. A. Sun, S. Pauly, J. Tan, M. Stoica, W. H. Wang, U. Kühn, and J. Eckert, Acta Mater. **60**, 4160 (2012).
[25] M. Lebyodkin, L. Dunin-Barkowskii, Y. Brêchet, Y. Estrin, and L. P. Kubin, Acta Mater. **48**, 2529 (2000).
[26] N. D. Denkov, S. Tcholakova, K. Golemanov, and A. Lips, Phys. Rev. Lett. **103**, 118302 (2009).
[27] D. Pan, A. Inoue, T. Sakurai, and M. W. Chen, Proc. Natl. Acad. Sci. U.S.A. **105**, 14769 (2008).
[28] P. Hähner and M. Zaiser, Acta Mater. **45**, 1067 (1997).

[29]M. S. Bharathi, M. Lebyodkin, G. Ananthakrishna, C. Fressengeas, and L. P. Kubin, Phys. Rev. Lett. **87**, 165508 (2001).

[30]W. L. Johnson, M. D. Demetriou, J. S. Harmon, M. L. Lind, and K. Samwer, MRS Bull. **32**, 644 (2007).

[31]W. L. Johnson and K. Samwer, Phys. Rev. Lett. **95**, 195501 (2005).

[32]M. D. Demetriou, J. S. Harmon, M. Tao, G. Duan, K. Samwer, and W. L. Johnson, Phys. Rev. Lett. **97**, 065502 (2006).

[33]P. E. Donovan, Acta Mater. **37**, 445 (1989).

[34]Z. F. Zhang and J. Eckert, Phys. Rev. Lett. **94**, 094301 (2005).

[35]F. Jiang, M. Q. Jiang, H. F. Wang, Y. L. Zhao, L. He, and J. Sun, Acta Mater. **59**, 2057 (2011).

[36]H. Q. Li, C. Fan, K. X. Tao, H. Choo, and P. K. Liaw, Adv. Mater. **18**, 752 (2006).

[37]B. Yang, M. L. Morrison, P. K. Liaw, R. A. Buchanan, G. Y. Wang, C. T. Liu, and M. Denda, Appl. Phys. Lett. **86**, 141904 (2005).

[38]X. H. Xu, G. Wang, F. J. Ke, and W. H. Wang, Scr. Mater. **59**, 657 (2008).

[39]G. Wang, X. H. Xu, F. J. Ke, and W. H. Wang, J. Appl. Phys. **104**, 073530 (2008).

[40]G. E. Dieter, *Mechanical Metallurgy*, 3rd ed. (McGraw Hill Companies, Inc., 2006).

[41]K. L. Johnson, *Contact Mechanics* (Cambridge University Press, 1985).

[42]Y. Tanaka, Y. Kawauchi, T. Kurokawa, H. Furukawa, T. Okajima, and J. P. Gong, Macromol. Rapid Commun. **29**, 1514 (2008).

[43]C. W. Parmelee, *Ceramic Glazes*, 3rd ed. (The Maple Press Company, 1973).